Journal of Materials Chemistry A

Accepted Manuscript

ROYAL SOCIETY OF CHEMISTRY

www.rsc.org/materialsA

Panchromatic Polymer-polymer Ternary Solar Cells Enhanced by Förster Resonance Energy Transfer and Solvent Vapor Annealing

Tenghooi Goh[1], Jing-Shun Huang[1,2], Benjamin Bartolome[1], Matthew Y. Sfeir[3], Michelle Vaisman[4], Minjoo Lee[4], and André D. Taylor[1]★

.KEYWORDS: P3HT; PTB7; Ternary Solar Cells; Energy Transfer; Solvent Annealing; Bulk-heterojunction; Polymer photovoltaics

Abstract

Thanks to the bulk-heterojunction (BHJ) feature of polymer solar cells (PSC), additional light active components can be added with ease to form ternary solar cells. This strategy has achieved great success largely due to expanded spectral response range and improved power conversion efficiency (PCE) without incurring excessive processing costs. Here, we report ternary blend polymer-polymer solar cells comprised of PTB7, P3HT, and $PC_{71}BM$ with PCE as high as 8.2%.

[1]Department of Chemical and Environmental Engineering, Yale University, New Haven, CT 06511, USA
[2]Currently in Thomas J. Watson Laboratories of Applied Physics, California Institute of Technology, Pasadena, CA 91125, USA
[3]Center for Functional Nanomaterials, Brookhaven National Laboratory, Upton, NY 11973, USA
[4]Department of Electrical Engineering, Yale University, New Haven, CT 06511, USA
★e-mail: andre.taylor@yale.edu

Analysis from femtosecond time resolved photoluminescence and transient absorption spectroscopy confirm that P3HT is effective in transferring energy non-radiatively by inducing excitons and prolonging their overall lifetime in PTB7. Furthermore, solvent vapor annealing (SVA) treatment has been employed to improve the overly-coarse surface morphology. As a result, the fill factor and interfacial recombination has been further improved, boosting the PCE to 8.7%.

Development in material synthesis especially on advanced low-bandgap copolymers has set a remarkable benchmark on the highest efficiency of over 10%[1-4]. Still, these reported records remain below the estimated ultimate efficiency limits of 14-21% for organic solar cells[5, 6]. Single-junction polymer solar cells (PSC) with only a single electron donor-acceptor pair are inevitably restricted by light absorption limitation because of the polymer excitonic characteristics[7]. Photon energy outside of the absorption range of the active component ends up being wasted in addition to other losses due to thermalization or exciton recombination.

To overcome these problems, ternary organic solar cells have emerged very recently as a simpler alternative to extend the sensitivity spectrum in OPV[8]. Thanks to the nature of the bulk-heterojunction structure employed in most of the organic solar cells, additional polymer[7], small molecule[9], quantum dots[10], or fullerene derivatives[11] can simply be mixed into the conventional binary layer, resulting in a more efficient ternary system with broad-band light harvesting. Among all, *poly(3-hexylthiophene-2,5-diyl)*, (P3HT) is arguably one of the most commonly studied candidates for organic ternary systems.[12-17] However, in many instances, additions of incompatible materials can result in lowered performances[18-24]. This incompatibility can be manifested in many ways[23, 25, 26], including competitive absorption, misaligned energy level configuration, non-miscibility, and morphological traps. Although some guidelines have been put forward in this emerging subject in PSC research, accurate theories and simulations are yet to be established[27].

PTB7, or *Poly([4,8-bis[(2-ethylhexyl)oxy]benzo[1,2-b:4,5-b']dithiophene-2,6-diyl][3-fluoro-2-[(2-ethylhexyl)carbonyl]thieno[3,4-b]thiophenediyl])*, has captured much attention for being one of the highest efficiency single-junction PSC in literature[28]. Composed of a polymer backbone of alternating thieno[3,4-b]thiophene and benzodithiophene units, PTB7 is the 7th generation in the series where the moiety groups were optimized for spectral coverage over the range of 550-700 nm, hole mobility, as well as fulleride miscibility[29]. In this work, we demonstrate the potential of ternary devices composed of P3HT and PTB7 blends as donors and *[6,6]-phenyl-C_{71}-butyric acid methyl ester* ($PC_{71}BM$) as an electron acceptor. A recent report from Y. Ohori et. al. suggested that the use of small amounts of P3HT in PTB7:$PC_{61}BM$ could function as a replacement of 1,8-diiodooctane (DIO), which is a common additive for improving the fill factor in conventional PTB7 based solar cells[30]. Here we show that the increased fill factor observed in this system are primarily based on optical enhancements derived via energy transfer. To the best of our knowledge, a systematic study of P3HT:PTB7:$PC_{71}BM$ inverted PSCs have not been previously reported in the literature.

Chemical structures and optical properties of P3HT, PTB7, and blend films.

We show the molecular structures of materials present in the active layer for this work (Fig. 1a-c). The molecular structural difference of these two polymers implies that their optoelectrical properties can be deviated in many ways. For example, P3HT comprises of single hexyl-thiophene monomer while PTB7 is a donor-acceptor (D-A) copolymer. Hence, P3HT exhibits a wider bandgap (~ 2.1 eV) compared to PTB7 (~ 1.7 eV)[31]. Despite this difference, H. Kim et. al. reported improved ternary cells containing wide- and narrow-bandgap polymers[18]. They

suggested that the key is to control the blending ratio to attain better control and balance of hole and electron transport properties. In addition, the energy levels between P3HT, PTB7, and $PC_{71}BM$ follow a cascade alignment (Fig. 1d), indicating that the incorporation of P3HT can lead to efficient charge transfer pathway[8, 30, 32].

A comparison of optical properties suggests that P3HT and PTB7 are complementary and not competing. P3HT exhibits a high absorption coefficient[33] over the blue–green visible spectrum (400-600 nm) whereas PTB7 absorbs primarily at the yellow-red spectrum (570 – 750 nm), thus implies that creating P3HT-PTB7 blends can be advantageous in broadening the total absorption window (Fig. 2a). This finding prompted us to further measure the optical absorption of films consisting of 1, 5, 10, and 20% of P3HT incorporated PTB7:$PC_{71}BM$ (1:1.5 weight ratio). As anticipated, films with moderate P3HT loading (5 and 10%) display a more well-rounded, or panchromatic coverage over the entire visible light spectrum (Fig. 2b).

Since both P3HT and PTB7 are chromophores, theoretically Förster resonance energy transfer (FRET) can be triggered when optical, electronic, and spatial conditions of the polymer blend are met[34]. As introduced in our previous work, FRET enhancement can increase the OPV efficiency by as much as 38%[35] and 46%[36] in dye-dye and polymer-dye ternary systems respectively. In fact, the presence of cascade structures in many biomolecular complexes enhances the efficacy of photosynthetic energy utilization by preventing recombination loss through energy transfer and inducing separation of charges[34]. A recent perspective from L. Yang *et. al.* also suggests that the benefits of ternary solar cells can be fulfilled by taking advantage of three fundamental mechanisms, namely charge transport, energy transfer and parallel linkage enhancement[32].

For a quick assessment on the likelihood of P3HT and PTB7 energy transfer, we investigated the steady-state photoluminescence (PL) characteristics. We first observe there is a great deal of overlap between the emission spectrum of P3HT and absorption of PTB7, satisfying one of the requirements for FRET to occur, as demonstrated in our previous works. We show the steady-state fluorescence studies of the P3HT-PTB7 films under 405 nm excitation wavelength (Fig. 2c). This wavelength was chosen to contrast the PL selectivity of P3HT over PTB7, although the PL of neat PTB7 is still observable. We infer that energy transfer occur between the P3HT and PTB7 due to (i) a noticeable decrease of the characteristic PL features of P3HT that peak at 650, 680, and 708 nm (corresponding to the 0-0, 1-0, 2-0 π^*- π transitions[37]), and (ii) the PL of PTB7 (λ_{max} at 760 nm) becomes stronger. As the P3HT concentration in mixed films increases, observations of the escalating magnitude of both quenching and sensitized emission is a strong indication that photon energy over this range can cause excitonic energy from the P3HT to be channeled towards the PTB7. In addition, we calculate the Förster radius (R_0), the theoretical distance at which energy transfer at 50% efficiency between chlorobenzene solvated P3HT and PTB7, to be c.a. 6.5 nm (*supporting information, S2*). We note that this lengthscale ($2\times R_0$) is comparable to the domain sizes obtained from AFM images (*vide infra*), inferring FRET is preferable in this intimately mixed system.

Photodynamics probed by time-resolved spectroscopy

We employed time-resolved photoluminescence (TRPL) to gain insights on the exciton recombination decay kinetics by studying PTB7 fluoresence. Using a low fluence pumping wavelength at 500 nm, we reveal the average PL time constant detected at 750 nm to be 27.4 ps in the neat PTB7 film. This number increases to 31.3 ps, 39.0 ps, and 54.1 ps for films with 1, 5, and 10% P3HT respectively (*supporting information*, S4). These results show that incorporation of P3HT helps prolong the intensity-independent recombination lifetime of excitons in the PTB7, according to FRET theory. To clarify, the time constants were obtained by fitting the decay profiles with three component-exponential Gaussian formula and averaging over the normalized amplitudes. These films were also prepared from solutions with the same amount of PTB7.

In order to understand photodynamic details for this sensitization process, we employ ultrafast transient absorption spectroscopy. We show the spectral- and time- resolved data detected at the visible range for the polymer-polymer films (Fig. 3). We ascribe the negative bands spanning from 550 nm to 770 nm that appear in all films predominantly to ground-state bleaching (GSB) of PTB7, and the peaks at 690 and 630 nm, as well as the shoulder at 560 nm represent the 0-0, 0-1, and 0-2 vibronic transitions respectively.

We show that for films with more P3HT, the GSB signal at 690 nm grows stronger at early time (< 50 ps) (Fig. 3 and Fig. *S3a-b*). Since the bleaching of the P3HT does not occur at this wavelength[35], the increase of GSB of PTB7 can be ascertained by non-radiative excitonic energy transfer from P3HT. To enumerate, we quantify the absolute intensity ($|\Delta A|$) of this peak at 1 ps in arbitrary unit. As the P3HT loading rises from 1% to 5% and 10%, this value also rises from 3×10^{-3} in neat PTB7 to 3.5, 3.8 and 4.2 $\times10^{-3}$ respectively (Fig. 3a-h). The kinetics (Fig. 3b, d, f, g) at 690 nm also reveals that the GSB lifetime of PTB7 gets prolonged. Meanwhile, the peak intensity at 630 nm remains approximately the same (only slightly higher for the 10% P3HT sample) at 1.9×10^{-3} regardless of whether P3HT is added or not. Together, these observations imply that the increasing bleaching signal of 0-0 PTB7 is in agreement with the energy transfer picture. In addition, we also observe that the peak at 560 nm surges in the blend with 10% P3HT only but not in the other blended samples. Since this peak corresponds very well to the GSB signal from neat P3HT (*supporting information*, Fig. *S3a-b*), this could mean that a film with a 10% loading starts to exhibit larger domains of P3HT, which in turn minimizes the PTB7 interface and hence favors its own bleaching.

Photovoltaic Performance

To investigate the photovoltaic performance of the P3HT-PTB7 devices, a series of P3HT-added PTB7:$PC_{71}BM$ devices were fabricated to study the dependency of the device performance on the composition ratio. We show the current density versus voltage measured under simulated AM 1.5 illumination at 100 mW cm^{-2} in figure 4a. Summarized in table 1 are the pertinent metrics as a function of P3HT loading. The control PTB7:$PC_{71}BM$ binary devices exhibit a typical PCE of 7.1%, comparable to the results of previous publications[31, 38, 39]. The introduction of P3HT into the PTB7:$PC_{71}BM$ (3% v/v DIO) matrix results in the enhancement in the J_{sc} as predicted by the optical enhancement. Remarkably, we reveal that devices with 5% P3HT records the highest efficiency among all as-casted ternary cells, reporting a PCE of 8.2%, J_{sc} of 17.1 mA/cm^2, V_{oc} of 0.72 V, and FF of 67%. Indeed, as addressed earlier, higher concentrations

of P3HT (>5%) leads to a reduction of device performance, which could originate from excessive blending of the "incompatible"[23] P3HT with the PTB7. We notice that all the as-casted ternary cells in this study suffer from a lower V_{oc} and FF compared to the control cells, and the magnitude of this decrease is proportional to the amount of P3HT added. The increasing J_{sc} counteracts this trend up to 10% P3HT loading, at which the average device efficiency drops to 6.4% with a V_{oc} of 0.62 V and a fill factor of 61.8%.

The improvement of J_{sc} is further elucidated by the results of external quantum efficiency (EQE) measurement. We analyze the results in figure 5a by breaking down the spectrum into two sections. First, the features in the 400 – 600 nm range are primarily associated with P3HT's absorption where the average EQE improves from 60.6%, to 64.8%, 68.4% and 71.3% (for 1, 5, and 10% P3HT cells respectively) in response to increasing P3HT concentration. As for the region at 600-750 nm, the photoresponse of the PTB7 is the predominant factor that affects the photocurrent output. Changes of the average EQE is less drastic. We observe only a slight increase from the control 76.6% to 77.1% (for 1% P3HT) and a plateau at 77.5% for devices with 5% and 10% P3HT loading. The EQE difference (ΔEQE) of the ternary films further validate that the major improvements that contribute to photocurrent come from 400 – 550 nm radiation (Fig. 5b).

In contrast, additional P3HT does generally not favor a higher V_{oc} and FF. The reduction of the V_{oc} could shed light on the orientation of the P3HT, PTB7, and $PC_{71}BM$ in the bulk. Often the V_{oc} of many un-doped single-layer ternary solar cells is located between the V_{oc} of the binary systems[18, 40-42]. The decreasing trend of the resultant V_{oc} (as P3HT insertion is increased) is consistent to typical P3HT:PCBM devices which reported values from 0.52 to 0.6 V[35, 43, 44]. Given that the interfacial layers and electrodes are the same, the V_{oc} of organic solar cells can be associated to the offset of the donor's highest occupied molecular orbital (HOMO) level and the fullerene's lowest occupied molecular orbital (LUMO)[45]. Therefore, we can infer that for 10% P3HT-added devices, the interface portion of the P3HT/$PC_{71}BM$ becomes prominent and thus produces more less-energetic electrons. If this is the case, some of the solutions to the problem of lowering the V_{oc} would be to: (i) use a higher HOMO polymer, or (ii) reduce (but not eliminate) the interface of the P3HT/$PC_{71}BM$ in favor of the PTB7/$PC_{71}BM$.

The FF decrease at higher concentrations of P3HT can be associated to the incompatible packing issue[2]. We correlate the FF drop to an increase in series resistance (R_s) and a decline of shunt resistance (R_{sh}) (Table 1). The R_s related to the interfacial resistance and low R_{sh} represents current leakage in the system[46]. A high R_s of the ternary devices implies the presence of recombination sites caused by a conflicting packing structure. Hence, understanding the morphological properties of ternary films especially at the organic/electrode interface is crucial[47], which leads us to the following investigation in the next section.

Study of Nano-morphology

Apart from the photonic behavior, it is equally important to address the morphological impact when P3HT and PTB7 are packed together. While individually, P3HT can be annealed to form a semi-crystalline film (favors 'edge-on' orientation thermodynamically)[48], PTB7 films take the form of a disordered amorphous (prefer 'face-on' and isotropic)[49] configuration. According to

extensive studies on multi-donor ternary solar cells by Y. Yang et. al., it is very likely that blending P3HT with PTB7 could result in "incompatible" ternary films as the insertion of 'edge-on' domains into 'face-on' microstructures can lead to the disruption of effective charge transfer pathways and induce recombination sites[23]; two factors that are identified to lower the FF[50].

We conducted tapping-mode atomic force microscopy (AFM) to characterize how the film topology behaves under the influence of additional polymer donor. The results of some typical 1 μm^2 screening windows under different compositions are displayed in Table 2. AFM was carried out on films that were spin-cast on annealed ZnO/Si wafers to better simulate the surface conformation of actual devices and analyzed with WSxM 5.0 software[51]. The film of binary control, PTB7:$PC_{71}BM$, exhibits a rather smooth and featureless morphology, with the domain size falling in the range of 10-50 nm, and is in agreement with work by G. J. Hedley et. al.[52] We attribute this observation to the solvent additive DIO in suppressing the phase separation of the polymer:fullerene blend. In contrast, the height profiles of the P3HT added ternary films show a steady increase in the root mean square (RMS) roughness. This number rises from 0.9 nm to 1.2 nm (for 1% P3HT), 1.9 nm (for 5% P3HT) and reaches 2.8 nm for samples with 10% P3HT. Notably, the formation of a slightly coarser surface can be favorable for higher efficiency BHJ photovoltaics[53, 54].

The phase and amplitude scans further unravel more information about homogeneity and probe-surface interaction. We note that when the P3HT loading is increased, the microfibrilar-like features that arise from the polythiophene become prominent, accompanied by larger domain sizes. This indicates that the presence of P3HT induces a large extent of unfavorable phase segregation between the polymer and fullerene compounds, and hence thwarts effective exciton dissociation.

Enhancement by solvent annealing

In view of the drawbacks inherited from mixing "incompatible"[23] polymers, we attempt to re-engineer the film properties by performing solvent vapor annealing (SVA) modification. Reportedly, thermal annealing can deteriorate the device performance of PTB7:$PC_{71}BM$ by encouraging overly large aggregation[55]. Carefully, we employ the SVA technique to improve the photovoltaic performance without introducing excessive heat. This method was also documented to effectively alter the surface conformation and interfacial properties for PSC enhancement[56-58]. Other non-chlorine based solvent vapors such as methanol had also been used to increase the performance of PTB7:$PC_{71}BM$ from 7.1 to 7.9% PCE[58-60].

We treated the 5% P3HT with chloroform-xylene co-solvent vapor for 4 hours under room temperature. We observe the as-casted 5% P3HT ternary samples, average PCE under AM1.5 illumination of treated cells increase from 8.14% to 8.63% (highest PCE among 6 cells is 8.72%) after the treatment. Interestingly, the enhanced PCE is associated to an increase of the FF to 69%, in particular, the sharp decline in the R_s (Fig. 4b and Table 1). This enhancement is attributed to reduced interfacial resistance, as substantiated by AFM results. As pointed out by other works on SVA, chloroform treatment has reported to increase crystallinity, reduce in-plane π-π stacking of the polymer backbone and domain size of polymer:fullerene phase segregation[61, 62].

We demonstrate that under the effect of chloroform, the SVA sample reveals smaller but more dispersed domains and the topology becomes less microfibrillar-like (Table 2).[57] As some modelling simulations suggest[63], these stratification phases in the as-casted films are formed due to the rapid shearing and drying process during spin-coating. We reveal that the slow drying process of SVA allows more time for the organics to self-orient at thermodynamically favorable conformation. In this case, SVA treatment could induce fullerene micro-ripening[64] and provide driving force for polymer to rearrange intimately[62] without causing adverse large-scale phase separation introduced by thermal annealing.

The EQE of the vapor-exposed films shows an overall up-shift of the spectrum with reference to the 5% P3HT ternary sample, indicating that enhancement by SVA is more likely to be electronic since the results do not show optical preference to any particular spectrum range. To correlate the microscopic mechanical changes to electronic properties, we fabricated hole-only devices and the mobility was analyzed by the space-charge limited current methodology[65, 66]. By solving the gradients and intercepts (Fig. 5c), we deduce that the hole mobilities are 9.92×10^{-4} (binary), 3.06×10^{-3} (5% P3HT), and 4.08×10^{-3} $cm^2V^{-1}s^{-1}$ (5% P3HT, solvent annealed). We note that the hole mobility of the PTB7:$PC_{71}BM$ control is comparable to $\sim 1\times 10^{-3}$ $cm^2V^{-1}s^{-1}$ reported elsewhere[67]. Increases in the hole-mobility by SVA has been associated to inhibition of space charges accumulated at the interfaces, thus leading to lower charge recombination and an increase of the FF[59].

To investigate the dominating recombination type, we survey the log-log plot of the J_{sc} versus illumination intensity (L). The lower value of fitted linear slope, α, from unity signifies the bimolecular recombination is stronger[68]. Following the relation of $J_{sc} \propto L^{\alpha}$, the power factor of illumination intensity on J_{sc} (α) for typical devices are 0.91 ($\alpha_{(binary)}$), 0.84 ($\alpha_{(1\%\ P3HT)}$), 0.86 ($\alpha_{(5\%\ P3HT)}$), and 0.89 ($\alpha_{(5\%\ P3HT\text{-}SVA)}$) respectively (Fig. 5d). These results reinforce our inferences that (1) initial incorporation of morphologically incompatible P3HT promotes recombination sites as $\alpha_{(1\%\ P3HT)} < \alpha_{(binary)}$; (2) comparing of results of 1% P3HT and 5% P3HT, $\alpha_{(5\%\ P3HT)} > \alpha_{(1\%\ P3HT)}$, FRET mechanism helps reducing bimolecular recombination loss at the optimal blending; and (3) SVA is effective in alleviating loss due to recombination with the increase of $\alpha_{(5\%\ P3HT\ SVA)}$ compared to $\alpha_{(5\%\ P3HT)}$ without post-treatment. These findings resonate with the theme of this paper that polymer compatibility should be taken into consideration when designing a new system for multi-donor solar cells and adopting multiple enhancement strategies can to facilitate the development of ternary photovoltaics research to greater heights.

Conclusion

To conclude, we report a simple yet effective method to produce high efficient ternary polymer-PSCs. We demonstrate that P3HT and PTB7 are optically complimentary and the mixed films enjoy benefits of panchromatic absorption coverage, cascaded energy alignment, and rapid energy transfer enhancement. However, structurally P3HT and PTB7 have distinctly different

preferred packing orientation, and as such this disruption leads to a drastic drop of the FF. To circumvent the problems of mixing "incompatible" polymers, we show that SVA modification of ternary solar cells can effectively improve the FF and carrier mobility, which translates to 22.5% PCE improvement in comparison to the binary PSCs. We also establish that the charge recombination is suppressed by both FRET and the SVA processes, as evident by hole mobility measurements as well as recombination dynamics extracted from the J_{sc} versus light intensity plot. All in all, these findings unravel properties of polymer based ternary films that help formulate better strategies towards commercialization of high efficiency solar cells.

Experimental Section

Device Fabrication

ITO-coated thin glasses with sheet resistance of ~7 Ω/□ were purchased from Zhuhai Kaivo Optoelectronics and patterned in-house with HCl. P3HT (4002EE grade, Rieke Metals), PTB7 (1-Materials), and $PC_{71}BM$ (Nano-C, 99+%) were purchased and stored in N_2-filled glovebox. ZnO nanoparticles was grown on the wet-cleaned and ozone treated ITO substrates by sol-gel method[69, 70] and baked at 150 °C for 15 minutes. Chlorobenzene (Sigma-Aldrich) was degassed and dehumidified before mixing with 3% DIO (Alfa-Aesar). PTB7:$PC_{71}BM$ (with and without P3HT) solutions were stirred at 60°C for 40 hours and casted at approximately 35-45°C. Solvent annealed devices were flipped and transferred into a sealed French-press (modified in-house) that were saturated with xylene:chloroform (70:30 v/v) mixed solvent. Films were naturally dried in glovebox for at least 30 minutes after such treatment. A gap of ~ 1" was initially kept between the solvent level and the percolation mesh at room temperature. 0.6 nm of MoO_3 and 110 nm of Ag were thermally evaporated at pressure ~ 10^{-7} torr to form the contact electrodes.

PCE, Hole Mobility, and EQE Characterization

After fabrication, devices were illuminated at 100 $mWcm^{-2}$ from solar simulator with AM 1.5G filters (PV Measurements). The illumination intensity was calibrated by a quartz windowed Newport calibrated Si solar cell. The active area of the device irradiated by the light was defined as 8 mm^2 by using a photomask, so no extra current outside of the defined area was collected. Current density–voltage (J–V) data were acquired via Keithley 2400 source measurement unit from which device parameters over the best 16 devices were calculated and averaged (6 devices for solvent annealing experiment). R_s is determined by the inversed slope at 1 V. For hole mobility tests, devices of ITO/MoO_x/Polymer:Fullerene/MoO_x/Au were fabricated accordingly. Positive-bias J-V measurements of these "hole-only devices" were run under dark condition with the Au electrode grounded. Illumination studies were performed by inserting optical density filter along the radiation pathway. The absorption spectra of dried films and solutions were obtained using a Varian Cary 3E UV-vis spectrophotometer, while the film and solution emissions were inspected with Spectra Suite (Ocean Optics) and RF-5310 fluorescence spectrophotometer (Shimadzu) respectively. EQE measurements were performed in air with silicon cell calibrated QEX7 system (PV Measurements) under zero bias.

Time-resolved PL and Transient Absorption Measurement

Broadband TA spectra were obtained using an amplified Ti:Sapphire laser system and optical parametric amplifier (OPA). Briefly, neat P3HT, P3HT-PTB7, and blended films (Spectra-Physics) were resonantly excited with ~100 fs laser pulses generated by the OPA at repetition rate of 80 MHz. Time-resolved absorption spectra are obtained using a femtosecond broadband supercontinuum probe pulse that is overlapped in time and space with the femtosecond pump pulse. The supercontinuum is produced by focusing a small portion of the amplified laser fundamental into a sapphire plate. Multiwave-length transient spectra are recorded using dual spectrometers (signal and reference) equipped with fast Si array detectors. In all our experiment, we keep the fluence value at 16 μJcm^{-2}. Chirping due to the different time zero from the array of visible light in white beam is corrected before the data is analyzed.

AFM and cross-section SEM, X-SEM Measurement

Si wafers were cleaved into 1.5 cm^2 sample size and cleaned before spin casting neat and blended films on top. ZnO was precoated before spin-coating the active layers on Si substrates. AFM was conducted on a Bruker (Digital Instruments) under tapping mode with reflective probes resonating at 150 kHz frequency. Samples for X-SEM (with the exact solar cell architecture on ITOs) were immersed in liquid nitrogen for 15 minutes, cleaved at the center, sputtered with 7 to 9 nm of chromium, and loaded into Hitachi SU-70 SEM for inspection.

Acknowledgement

The authors gratefully acknowledge the National Science Foundation (DMR-1410171) and the NASA (CT Space Grant Consortium) for partial support of this work. A.T. also acknowledges support from the NSF-CAREER award (CBET-0954985). B.B. acknowledges support from the *Edward A. Bouchet-Robertson Fellowship.* The authors would like to express gratitude to Dr. Chuanhao Li and Professor Jaehong Kim for aiding measurements of solution photoluminescence, as well as Ms. Di Huang from Key Laboratory of Luminescence and Optical Information, Beijing Jiaotong University for discussion. This research was carried out in part at the Center for Functional Nanomaterials, Brookhaven National Laboratory, which is supported by the U.S. Department of Energy, Office of Basic Energy Sciences, under Contract No. DE-AC02-98CH10886. Facilities used was supported by YINQE and NSF MRSEC DMR 1119826 (CRISP).

Figure captions:

Figure 1 | Chemical structures and energy level of active materials. Showing here are the monomer unit of **a**, P3HT, **b**, PTB7, and **c** $PC_{71}BM$, **d**, theorectical HOMO and LUMO of the components of the ternary blend solar cell where three pathways of charge and energy transfer are highlighted. For the ease of simplicity, the mixed PTB7 and P3HT films are depicted as individual layer in the schematic representation.

Figure 2 | Optical properties of P3HT and PTB7. a, Chemical structures of P3HT and P3HT-PTB7. **b**, Normalized absorption of thermally evaporated thin films of P3HT-PTB7 (red), P3HT (blue), and C60 (black) on left axis; with the overlay of P3HT-PTB7 emission (red dot) spectra when excited by 500 nm on right axis. **c**, Steady state photoluminescence (PL) spectra and quenching of P3HT-PTB7:P3HT co-deposited films under a variation of blending ratio when excited by 405 nm laser.

Figure 3 | Photophysics study. a, Transient absorption spectrum traces of neat P3HT-PTB7 binary film, **c**, 1%. **e**, 5%. **g**, 10% P3HT incorporated PTB7:P3HT blend films in 1, 5, 10, 100, and 500 ps after time zero, while **b**, **d**, **f**, **g**, are the corresponding kinetics detected at 562 nm, 612 nm, 690 nm, and 726 nm. All films are casted from blended solutions under the same spin-rate.

Figure 4 | Solar cells performance: Impact of blending ratio. a, The J-V curves of the photovoltaic devices with the P3HT concentrations ranging from 0 to 5wt%. under 100 $mWcm^{-2}$ AM 1.5G irradiation, all devices contain 3% v/v DIO. **b**, Comparison of J-V curves for cells before and after SVA treatment. **c**, Schematic of inverted solar cells construction for J-V measurement. **d**, "Edge-on" and "face-on" configuration preference exhibited in P3HT and PTB7 respectively.

Figure 5 | EQE and electronic properties. a, External quantum efficiency (EQE) versus wavelength of the devices with the P3HT concentrations ranging from 0 to 10 wt%., and 5 wt% P3HT ternary cells with SVA treatment. **b**, EQE difference of ternary, and solvent-annealed ternary cells normalized to EQE of binary device. **c**, Hole mobility estimation of binary, 5 wt% P3HT, and SVA-modified 5 wt% P3HT ternary hole-only devices by SCLC method. **d**, Log-log plot of J_{sc} versus light intensity, L. The linearly best fitted slopes, α, were analyzed for recombination dynamics studies.

Table caption:

Table 1. Summary of photovoltaic parameters and efficiencies of solar cells variation of P3HT and PTB7 mixing ratio. All devices are prepared from the same stock solution, *i.e.* dehydrated chlorobenzene with 3% DIO v/v.

Blend Ratio	V_{oc} (V)	J_{sc} (mA/cm2)	FF (%)	Best PCE (%)	Mean PCE (%)	R_{sh} (Ω/cm2)	R_s (Ω/cm2)
Control PTB7:PCBM (Binary)	0.746	14.84	69.2	7.35	7.08	1174.35	0.34
Ternary 1% P3HT	0.731	15.62	67.1	7.67	7.44	763.86	0.50
Ternary 5% P3HT	0.721	17.10	66.6	8.22	8.14	562.76	0.45
Ternary 5% P3HT w/SVA	0.720	17.25	69.7	8.72	8.63	896.17	0.35
Ternary 10% P3HT	0.621	17.65	61.8	6.78	6.39	445.82	0.50

Table 2. Tapping mode AFM images of binary and ternary films with various P3HT loadings, as well as film with SVA treatment. All films were spin-casted from solutions with 3% v/v DIO additive.

	Height	Phase	Amplitude
PTB7:$PC_{71}BM$	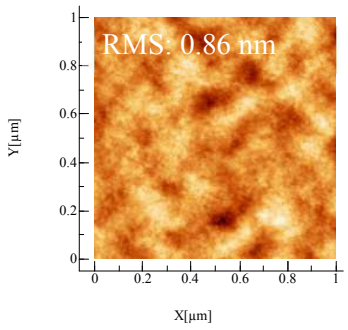	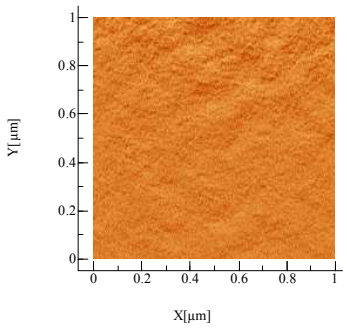	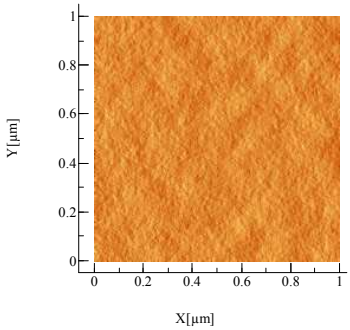
w/ 1% P3HT	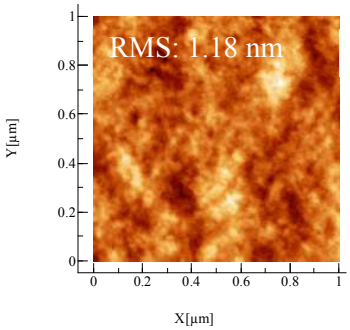	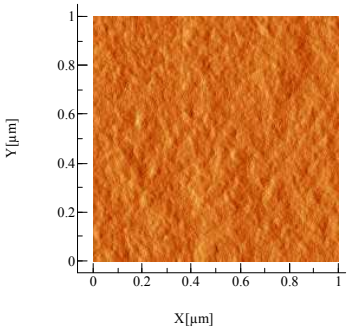	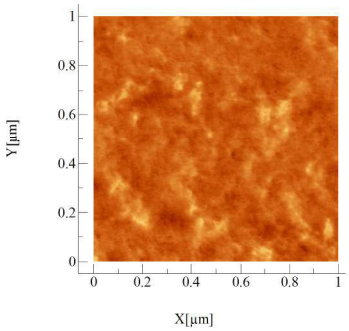
w/ 5% P3HT	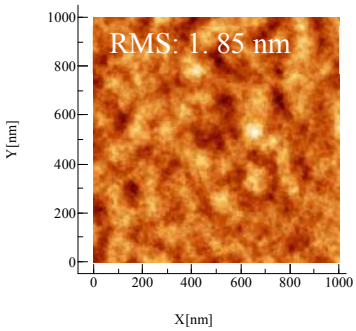	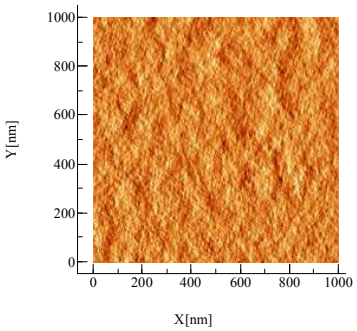	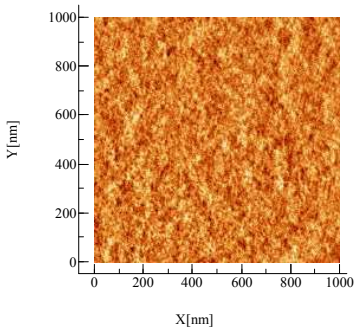

w/ 5% P3HT (SVA)	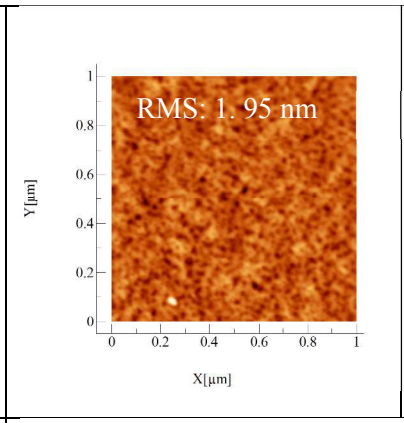	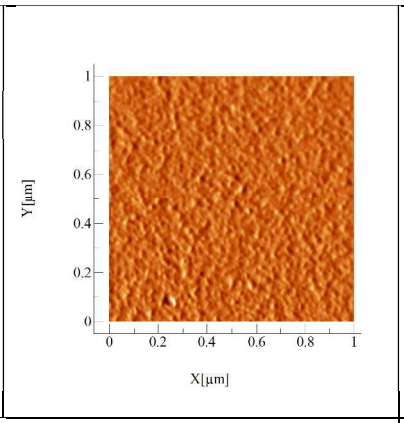	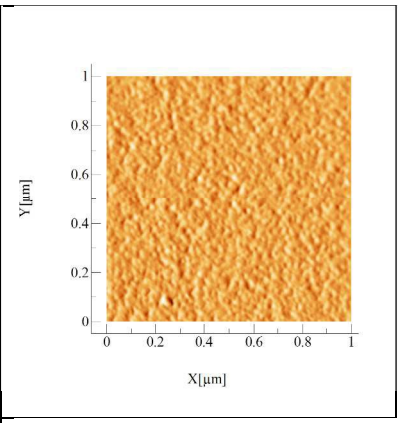
w/ 10% P3HT	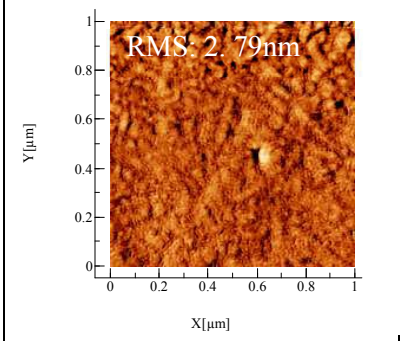	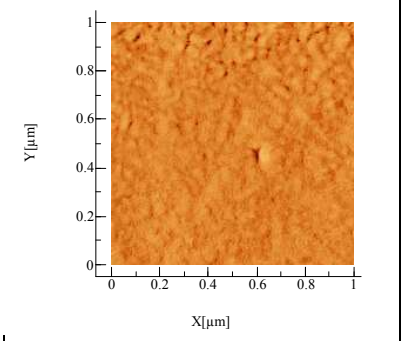	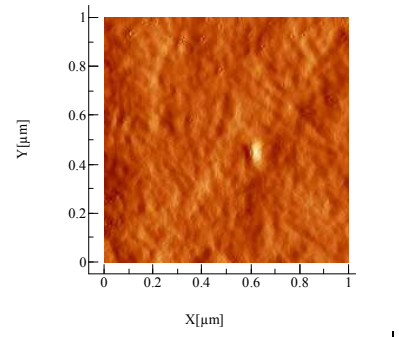
Sccale bars	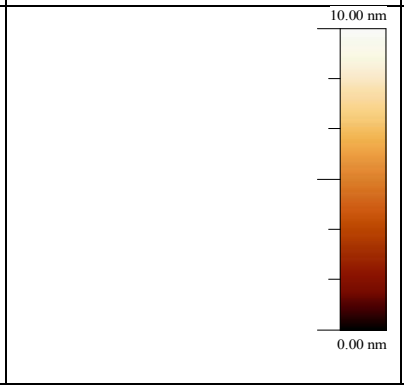	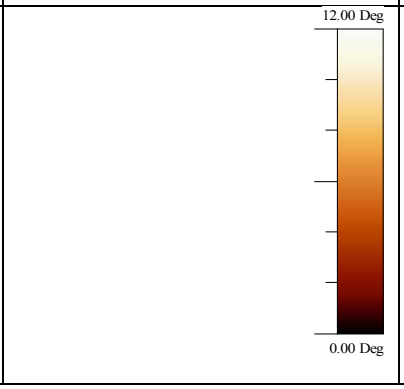	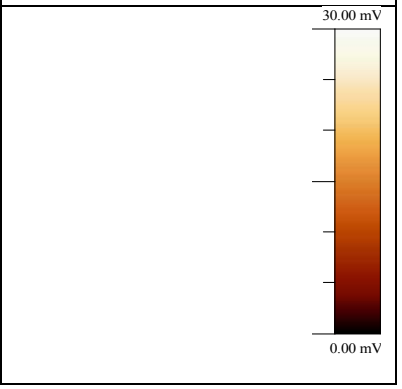

References

1. Z. He, C. Zhong, S. Su, M. Xu, H. Wu and Y. Cao, *Nature Photon.*, 2012, 6, 593-597.
2. X. Guo, N. Zhou, S. J. Lou, J. Smith, D. B. Tice, J. W. Hennek, R. P. Ortiz, J. T. L. Navarrete, S. Li, J. Strzalka, L. X. Chen, R. P. H. Chang, A. Facchetti and T. J. Marks, *Nature Photon.*, 2013, 7, 825-833.
3. L. Dou, W.-H. Chang, J. Gao, C.-C. Chen, J. You and Y. Yang, *Adv. Mater.*, 2013, 25, 825-831.
4. J. You, L. Dou, K. Yoshimura, T. Kato, K. Ohya, T. Moriarty, K. Emery, C.-C. Chen, J. Gao, G. Li and Y. Yang, *Nat. Commun.*, 2013, 4, 1446.
5. T. Kirchartz, K. Taretto and U. Rau, *J. Phys. Chem. C*, 2009, 113, 17958-17966.
6. M. C. Scharber and N. S. Sariciftci, *Prog. Polym. Sci.*, 2013, 38, 1929-1940.
7. T. Ameri, T. Heumuller, J. Min, N. Li, G. Matt, U. Scherf and C. J. Brabec, *Energy Environ. Sci.*, 2013, 6, 1796-1801.
8. Y.-C. Chen, C.-Y. Hsu, R. Y.-Y. Lin, K.-C. Ho and J. T. Lin, *ChemSusChem*, 2013, 6, 20-35.
9. Y. J. Cho, J. Y. Lee, B. D. Chin and S. R. Forrest, *Org. Electron.*, 2013, 14, 1081-1085.
10. H. Choi, J.-P. Lee, S.-J. Ko, J.-W. Jung, H. Park, S. Yoo, O. Park, J.-R. Jeong, S. Park and J. Y. Kim, *Nano Lett.*, 2013, 13, 2204-2208.
11. Y.-J. Cheng, C.-H. Hsieh, Y. He, C.-S. Hsu and Y. Li, *J. Am. Chem. Soc.*, 2010, 132, 17381-17383.
12. J. M. Lobez, T. L. Andrew, V. Bulović and T. M. Swager, *ACS Nano*, 2012, 6, 3044-3056.
13. J.-H. Huang, M. Velusamy, K.-C. Ho, J.-T. Lin and C.-W. Chu, *J. Mater. Chem.*, 2010, 20, 2820-2825.
14. S. S. Sharma, G. D. Sharma and J. A. Mikroyannidis, *Sol. Energy Mater. Sol. Cells*, 2011, 95, 1219-1223.
15. G. D. Sharma, S. P. Singh, M. S. Roy and J. A. Mikroyannidis, *Org. Electron.*, 2012, 13, 1756-1762.
16. Z. Hu, S. Tang, A. Ahlvers, S. I. Khondaker and A. J. Gesquiere, *Appl. Phys. Lett.*, 2012, 101, 053308.
17. J. Lee, M. H. Yun, J. Kim, J. Y. Kim and C. Yang, *Macromol. Rapid Commun.*, 2012, 33, 140-145.
18. H. D. Kim, H. Ohkita, H. Benten and S. Ito, *ACS Appl. Mater. Interfaces*, 2014, 6, 17551-17555.
19. F. Machui, S. Rathgeber, N. Li, T. Ameri and C. J. Brabec, *J. Mater. Chem.*, 2012, 22, 15570-15577.
20. N. Cooling, K. B. Burke, X. Zhou, S. J. Lind, K. C. Gordon, T. W. Jones, P. C. Dastoor and W. J. Belcher, *Sol. Energy Mater. Sol. Cells*, 2011, 95, 1767-1774.
21. M. Lv, M. Lei, J. Zhu, T. Hirai and X. Chen, *ACS Appl. Mater. Interfaces*, 2014, 6, 5844-5851.
22. H. Kang, K.-H. Kim, T. E. Kang, C.-H. Cho, S. Park, S. C. Yoon and B. J. Kim, *ACS Appl. Mater. Interfaces*, 2013, 5, 4401-4408.
23. Y. Yang, W. Chen, L. Dou, W.-H. Chang, H.-S. Duan, B. Bob, G. Li and Y. Yang, *Nature Photon.*, 2015, 9, 190-198.

24. H. Kim, M. Shin and Y. Kim, *J. Phys. Chem. C*, 2009, 113, 1620-1623.
25. N. J. Alley, K.-S. Liao, E. Andreoli, S. Dias, E. P. Dillon, A. W. Orbaek, A. R. Barron, H. J. Byrne and S. A. Curran, *Synt. Met.*, 2012, 162, 95-101.
26. A. Gusain, V. Saxena, P. Veerender, P. Jha, S. P. Koiry, A. K. Chauhan, D. K. Aswal and S. K. Gupta, *AIP Conf. Proc.*, 2013, 1512, 776.
27. T. Ameri, P. Khoram, J. Min and C. J. Brabec, *Adv. Mater.*, 2013, 25, 4245-4266.
28. Z. He, C. Zhong, S. Su, M. Xu, H. Wu and Y. Cao, *Nature Photon.*, 2012, 6, 591-595.
29. Y. Liang, D. Feng, Y. Wu, S.-T. Tsai, G. Li, C. Ray and L. Yu, *J. Am. Chem. Soc.*, 2009, 131, 7792-7799.
30. O. Yurina, F. Shunjiro, K. Hiromichi and N. Yasushiro, *Jpn. J. Appl. Phys.*, 2015, 54, 04DK09.
31. Y. Liang, Z. Xu, J. Xia, S.-T. Tsai, Y. Wu, G. Li, C. Ray and L. Yu, *Adv. Mater.*, 2010, 22, E135-E138.
32. L. Yang, L. Yan and W. You, *J. Phys. Chem. Lett.*, 2013, 4, 1802-1810.
33. S. Cook, A. Furube and R. Katoh, *Energy Environ. Sci.*, 2008, 1, 294-299.
34. R. E. Blankenship, *Molecular Mechanisms of Photosynthesis*, Blackwell Science, 1 edn., 2002.
35. J.-S. Huang, T. Goh, X. Li, M. Y. Sfeir, E. A. Bielinski, S. Tomasulo, M. L. Lee, N. Hazari and A. D. Taylor, *Nature Photon.*, 2013, 7, 479-485.
36. T. Goh, J.-S. Huang, E. A. Bielinski, B. A. Thompson, S. Tomasulo, M. L. Lee, M. Y. Sfeir, N. Hazari and A. D. Taylor, *ACS Photonics*, 2015, 2, 86-95.
37. Y. Zhang, T. P. Basel, B. R. Gautam, X. Yang, D. J. Mascaro, F. Liu and Z. V. Vardeny, *Nat. Commun.*, 2012, 3, 1043.
38. C. Liu, C. Yi, K. Wang, Y. Yang, R. S. Bhatta, M. Tsige, S. Xiao and X. Gong, *ACS Appl. Mater. Interfaces*, 2015, 7, 4928-4935.
39. S. Foster, F. Deledalle, A. Mitani, T. Kimura, K.-B. Kim, T. Okachi, T. Kirchartz, J. Oguma, K. Miyake, J. R. Durrant, S. Doi and J. Nelson, *Adv. Energy Mater.*, 2014, 4, 1400311-1400323.
40. L. Lu, T. Xu, W. Chen, E. S. Landry and L. Yu, *Nature Photon.*, 2014, 8, 716-722.
41. P. P. Khlyabich, A. E. Rudenko, R. A. Street and B. C. Thompson, *ACS Appl. Mater. Interfaces*, 2014, 6, 9913-9919.
42. K. Lu, J. Fang, X. Zhu, H. Yan, D. Li, C. a. Di, Y. Yang and Z. Wei, *New J. Chem.*, 2013, 37, 1728-1735.
43. G. Li, V. Shrotriya, J. Huang, Y. Yao, T. Moriarty, K. Emery and Y. Yang, *Nat. Mater.*, 2005, 4, 864-868.
44. D. Chen, A. Nakahara, D. Wei, D. Nordlund and T. P. Russell, *Nano Lett.*, 2011, 11, 561-567.
45. M. C. Scharber, D. Mühlbacher, M. Koppe, P. Denk, C. Waldauf, A. J. Heeger and C. J. Brabec, *Adv. Mater.*, 2006, 18, 789-794.
46. B. Qi and J. Wang, *Phys. Chem. Chem. Phys.*, 2013, 15, 8972-8982.
47. Z. a. Tan, S. Li, F. Wang, D. Qian, J. Lin, J. Hou and Y. Li, *Sci. Rep.*, 2014, 4.
48. *P3HT Revisited – From Molecular Scale to Solar Cell Devices*, Springer-Verlag Berlin Heidelberg, 2014.
49. B. A. Collins, Z. Li, J. R. Tumbleston, E. Gann, C. R. McNeill and H. Ade, *Adv. Energy Mater.*, 2013, 3, 65-74.

50. D. Bartesaghi, I. d. C. Perez, J. Kniepert, S. Roland, M. Turbiez, D. Neher and L. J. A. Koster, *Nat Commun*, 2015, 6.
51. I. Horcas, R. Fernández, J. M. Gómez-Rodríguez, J. Colchero, J. Gómez-Herrero and A. M. Baro, *Rev. Sci. Instrum.*, 2007, 78, 013705.
52. G. J. Hedley, A. J. Ward, A. Alekseev, C. T. Howells, E. R. Martins, L. A. Serrano, G. Cooke, A. Ruseckas and I. D. W. Samuel, *Nat. Commun.*, 2013, 4.
53. F.-C. Chen, H.-C. Tseng and C.-J. Ko, *Appl. Phys. Lett.*, 2008, 92, 103316.
54. Y. Yao, J. H. Hou, Z. Xu, G. Li and Y. Yang, *Adv. Funct. Mater.*, 2008, 18, 1783-1789.
55. F. Liu, W. Zhao, J. R. Tumbleston, C. Wang, Y. Gu, D. Wang, A. L. Briseno, H. Ade and T. P. Russell, *Adv. Energy Mater.*, 2014, 4, 1301377-1301386.
56. G. Li, Y. Yao, H. Yang, V. Shrotriya, G. Yang and Y. Yang, *Adv. Funct. Mater.*, 2007, 17, 1636-1644.
57. G. De Luca, E. Treossi, A. Liscio, J. M. Mativetsky, L. M. Scolaro, V. Palermo and P. Samori, *J. Mater. Chem.*, 2010, 20, 2493-2498.
58. Y. Zheng, S. Li, D. Zheng and J. Yu, *Org. Electron.*, 2014, 15, 2647-2653.
59. H. Zhou, Y. Zhang, J. Seifter, S. D. Collins, C. Luo, G. C. Bazan, T.-Q. Nguyen and A. J. Heeger, *Adv. Mater.*, 2013, 25, 1646-1652.
60. J. Yu, Y. Zheng and J. Huang, *Polymers*, 2014, 6, 2473.
61. J. Jo, S.-S. Kim, S.-I. Na, B.-K. Yu and D.-Y. Kim, *Adv. Funct. Mater.*, 2009, 19, 866-874.
62. E. Verploegen, C. E. Miller, K. Schmidt, Z. Bao and M. F. Toney, *Chem. Mater.*, 2012, 24, 3923-3931.
63. S. Y. Heriot and R. A. L. Jones, *Nat. Mater.*, 2005, 4, 782-786.
64. T. A. Bull, L. S. C. Pingree, S. A. Jenekhe, D. S. Ginger and C. K. Luscombe, *ACS Nano*, 2009, 3, 627-636.
65. P. Cheng, Y. Li and X. Zhan, *Energy Environ. Sci.*, 2014, 7, 2005-2011.
66. D. Huang, Y. Li, Z. Xu, S. Zhao, L. Zhao and J. Zhao, *Phys. Chem. Chem. Phys.*, 2015, 17, 8053-8060.
67. B. Ebenhoch, S. A. J. Thomson, K. Genevičius, G. Juška and I. D. W. Samuel, *Org. Electron.*, 2015, 22, 62-68.
68. I. Riedel, J. Parisi, V. Dyakonov, L. Lutsen, D. Vanderzande and J. C. Hummelen, *Adv. Funct. Mater.*, 2004, 14, 38-44.
69. Z. Liang, Q. Zhang, O. Wiranwetchayan, J. Xi, Z. Yang, K. Park, C. Li and G. Cao, *Advanced Functional Materials*, 2012, 22, 2194-2201.
70. J.-S. Huang, C.-Y. Chou and C.-F. Lin, *IEEE electron device letters*, 2010, 31, 332-334.

TOC Figure

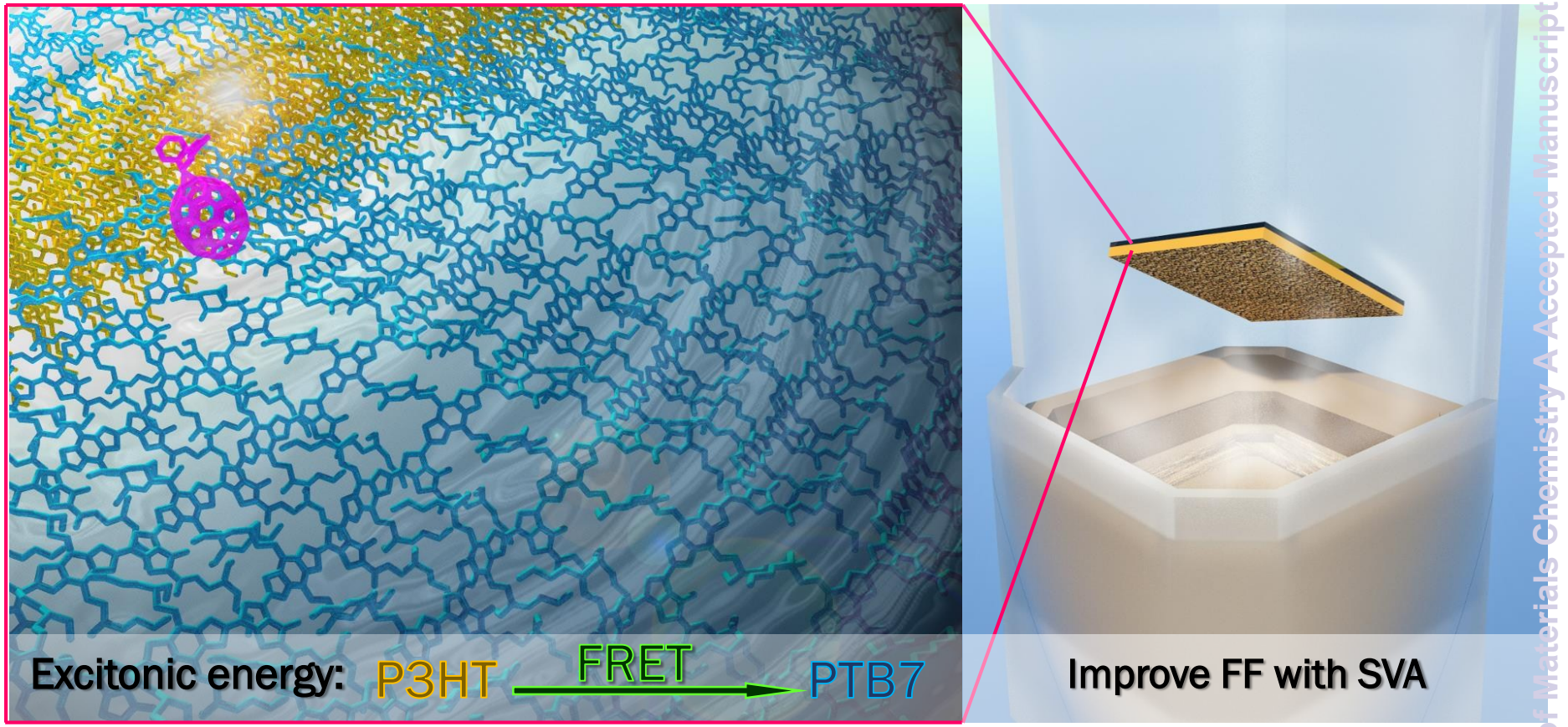

Figure 1

a

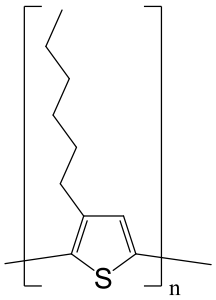

P3HT

b

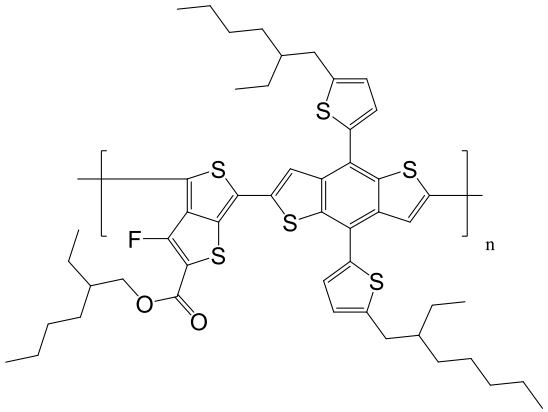

PTB7

c

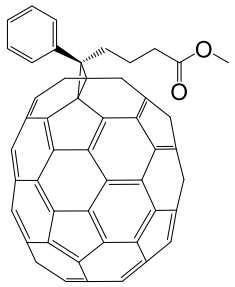

$PC_{71}BM$

d

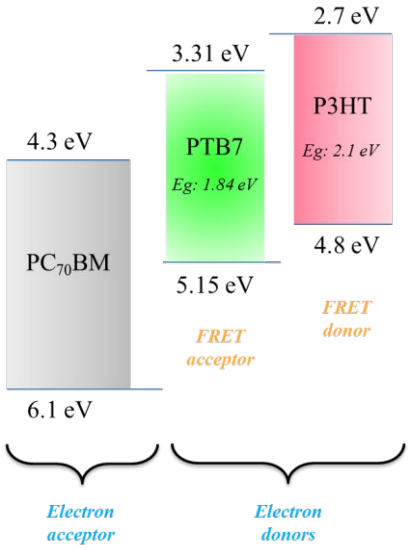

Figure 2

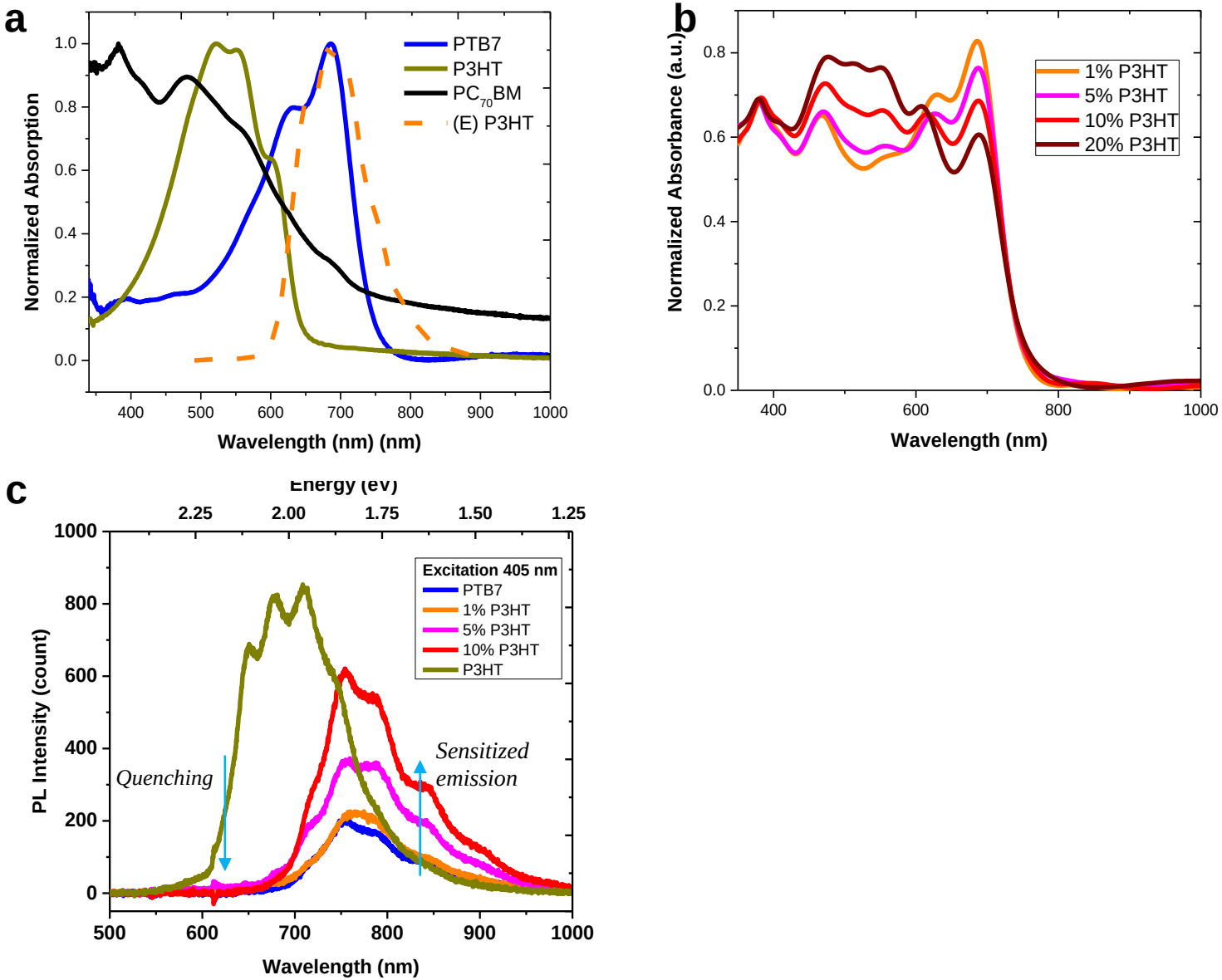

Figure 3

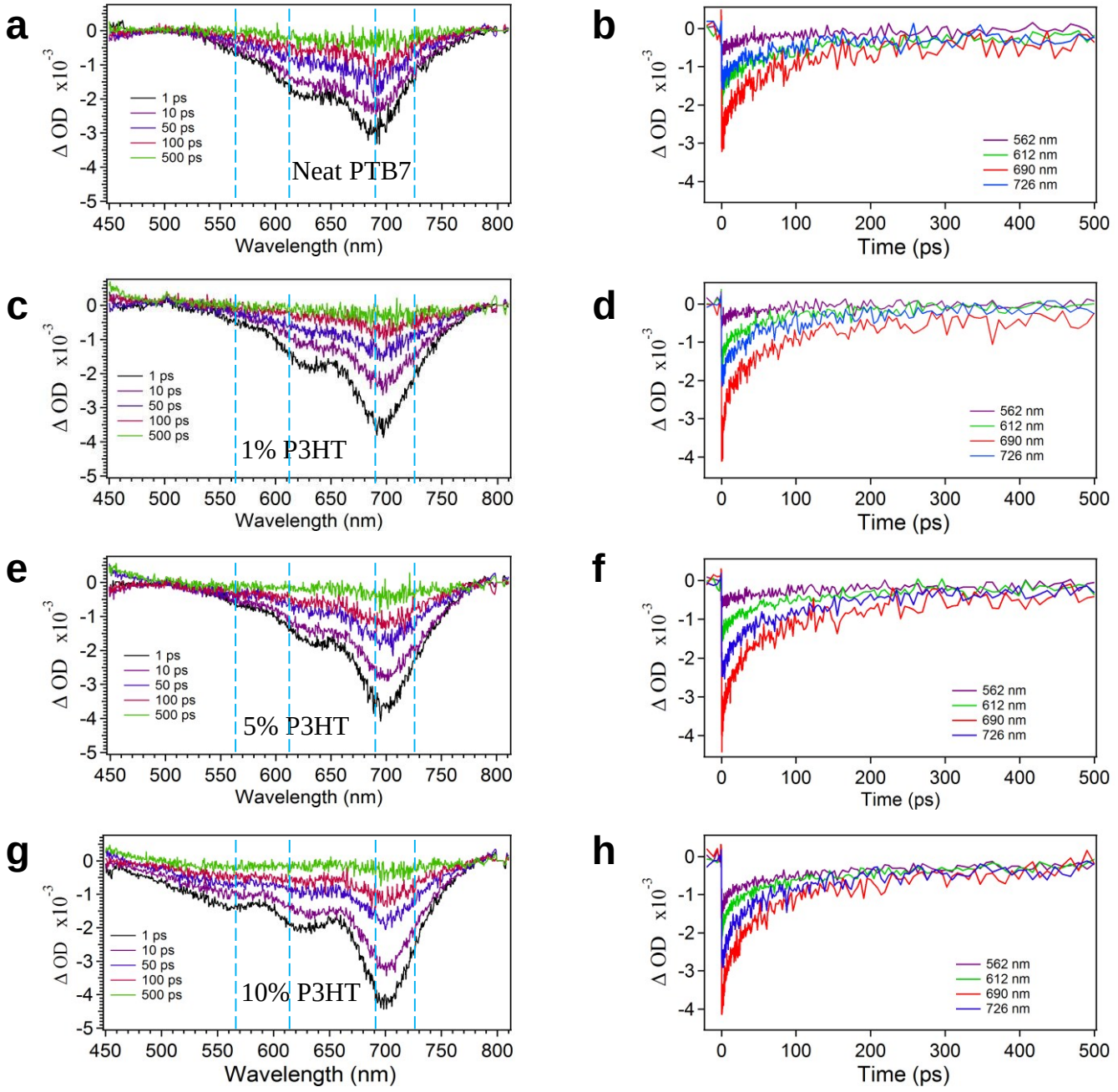

Figure 4

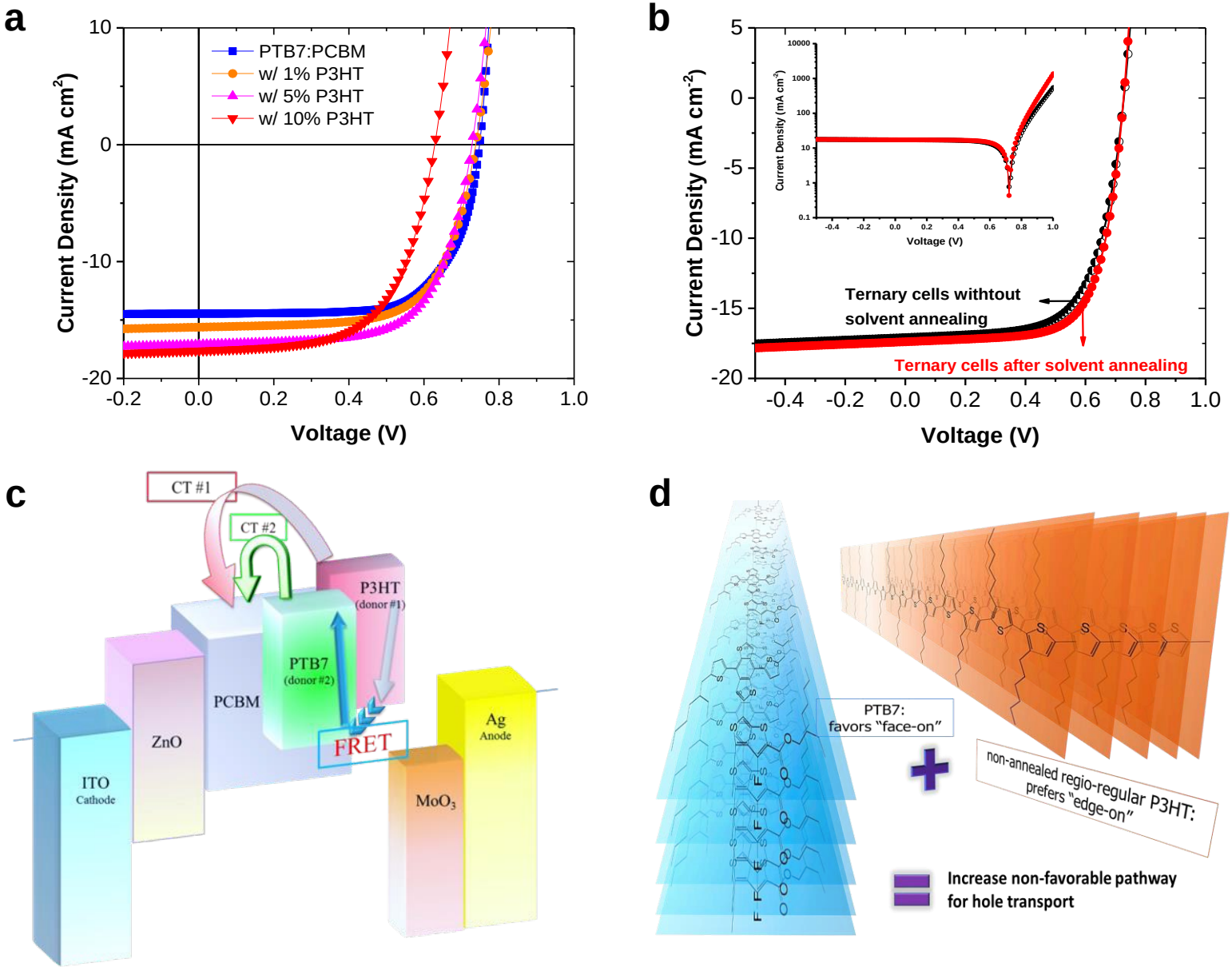

Figure 5